

## An Ionically Based Mapping Model with Memory for Cardiac Restitution

David G. Schaeffer<sup>a,d,\*</sup>, John W. Cain<sup>a</sup>, Daniel J. Gauthier<sup>b,c,d</sup>,  
Soma S. Kalb<sup>c</sup>, Robert A. Oliver<sup>c</sup>, Elena G. Tolkacheva<sup>b</sup>,  
Wenjun Ying<sup>a</sup>, Wanda Krassowska<sup>c,d</sup>

<sup>a</sup>Department of Mathematics, Duke University, Durham, North Carolina 27708, USA

<sup>b</sup>Department of Physics, Duke University, Durham, North Carolina 27708, USA

<sup>c</sup>Department of Biomedical Engineering, Duke University, Durham, North Carolina 27708, USA

<sup>d</sup>Center for Nonlinear and Complex Systems, Duke University, Durham, North Carolina 27708, USA

Received: 3 May 2005 / Accepted: 23 February 2006 / Published online: 20 January 2007  
© Society for Mathematical Biology 2007

**Abstract** Many features of the sequence of action potentials produced by repeated stimulation of a patch of cardiac muscle can be modeled by a 1D mapping, but not the full behavior included in the restitution portrait. Specifically, recent experiments have found that (i) the dynamic and S1–S2 restitution curves are different (rate dependence) and (ii) the approach to steady state, which requires many action potentials (accommodation), occurs along a curve distinct from either restitution curve. Neither behavior can be produced by a 1D mapping. To address these shortcomings, ad hoc 2D mappings, where the second variable is a “memory” variable, have been proposed; these models exhibit qualitative features of the relevant behavior, but a quantitative fit is not possible. *In this paper we introduce a new 2D mapping and determine a set of parameters for it that gives a quantitatively accurate description of the full restitution portrait measured from a bullfrog ventricle.* The mapping can be derived as an asymptotic limit of an idealized ionic model in which a generalized concentration acts as a memory variable. This ionic basis clarifies how the present model differs from previous models. The ionic basis also provides the foundation for more extensive cardiac modeling: e.g., constructing a PDE model that may be used to study the effect of memory on propagation. The fitting procedure for the mapping is straightforward and can easily be applied to obtain a mathematical model for data from other experiments, including experiments on different species.

---

\*Corresponding author.

E-mail addresses: dgs@math.duke.edu (David G. Schaeffer), jwcain@vcu.edu (John W. Cain).

## 1. Introduction

### 1.1. Preliminary concepts

Sudden cardiac death kills half of all people who die of heart disease, the Number One cause of death in the United States. ([http://www.hrspatients.org/patients/heart\\_disorders/cardiac\\_arrest/default.asp](http://www.hrspatients.org/patients/heart_disorders/cardiac_arrest/default.asp).) As part of a larger effort to understand and prevent fatal arrhythmias, much work has been devoted to studying the restitution properties of cardiac tissue under repeated stimulation, especially rapid stimulation (Hall et al., 1999; Banville and Gray, 2002; Fox et al., 2002b; Cherry and Fenton, 2004). In this paper, we attempt to reproduce in-vitro experiments that are conducted with small pieces of paced tissue, where the pacing rate is changed and the resulting responses measured.

When a small piece of cardiac muscle is subjected to a sequence of brief electrical stimuli whose strength exceeds a critical threshold, the myocytes respond by producing action potentials. Figure 1 shows a sketch of the transmembrane voltage measured from a single myocyte. Following a stimulus, the voltage first rises rapidly (indicating cell depolarization), then it has a plateau region during which the cell cannot be reactivated (the refractory period), and finally the voltage returns to its resting value (the cell repolarizes). This time course is known as an action potential. The interval between the time when the cell repolarizes following an action potential and the time when it depolarizes again (due to the next stimulus) is known as the diastolic interval. In this paper, the following acronyms<sup>1</sup> are sometimes used to refer to these concepts: APD, action potential duration; DI, diastolic interval; and BCL, basic cycle length or interval between stimuli.

For a periodic train of stimuli delivered at a slow rate, the myocytes display a phase-locked 1:1 response, where each stimulus produces an identical action potential. At faster pacing rates, the 1:1 response pattern is sometimes replaced by a 2:2 phase-locked period-2 response pattern, known as alternans. At even faster pacing rates, either the 1:1 or 2:2 response becomes unstable and is replaced by a 2:1 response pattern, where only every other stimulus elicits an action potential.

A fundamental characteristic of cardiac cells is the shortening of APD's as the pacing rate increases, known as *electrical restitution*. To model this behavior, Nolasco and Dahlen (1968) proposed the approximation<sup>2</sup>

$$A_{n+1} = G(D_n) \tag{1}$$

where  $A_n$  denotes the duration of the  $n$ th action potential,  $D_n$  denotes the duration of the  $n$ th diastolic interval, and  $G(D)$  is a monotone-increasing function of the diastolic interval. If  $B$  denotes the BCL with which the stimuli are applied, then  $D_n = B - A_n$ . Substituting into (1), we see that in this model the sequence  $A_n$  is determined recursively by iteration of a 1D map.

<sup>1</sup>When mathematical notation is intended, the notation is shortened to  $A$ ,  $D$ , or  $B$ , respectively.

<sup>2</sup>Strictly speaking, Eq. (1) holds only if the DI exceeds a certain threshold. See the Appendix for a discussion of how the imposition of such a threshold leads to 2:1 and higher-order responses.

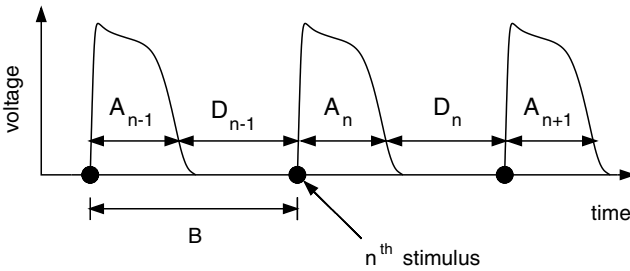


**Fig. 1** Schematic action potentials, showing action potential duration ( $A_n$ ), diastolic interval ( $D_n$ ), and basic cycle length ( $B$ ).

According to (1), under any pacing protocol, pairs of points ( $D_n, A_{n+1}$ ) would lie on a single curve, the graph of the function  $G(D)$  in the  $D, A$ -plane, what cardiologists would call the restitution curve. However, as pointed out by Elharrar and Surawicz (1983), restitution behavior depends on the protocol used in its measurement, often referred to as *rate-dependence* or *memory*. In this paper we focus on the following protocols, as described in detail in Kalb et al. (2004) and briefly here:

- (i) In the *dynamic protocol*, the tissue is paced periodically with period  $B$  until the tissue reaches steady state, and the steady-state action potential duration  $A_{ss}$  and diastolic interval  $D_{ss}$  are measured. The pacing period  $B$  is changed and the procedure is repeated, many times. The pairs of points ( $D_{ss}, A_{ss}$ ) form the dynamic restitution curve.
- (ii) In the *S1–S2 protocol*, the tissue is also paced periodically with period  $B$  (the “S1” stimuli in “S1–S2”) until the tissue reaches steady state. Then, say at  $n = N + 1$ , a sudden change is made in the pacing period (the “S2” stimulus). The diastolic interval  $D_N$  preceding the S2 stimulus and the resulting action potential duration  $A_{N+1}$  are recorded. The procedure is repeated for various S2 intervals, and the pairs of points ( $D_N, A_{N+1}$ ) form *one* of the S1–S2 restitution curves. There is a different S1–S2 restitution curve for each value of S1, a characteristic of rate-dependent restitution.
- (iii) The *perturbed-downsweep protocol* (Kalb et al., 2004) combines data about both dynamic and S1–S2 restitution, as well as information about the transients in the approach to steady state. This information is conveniently summarized in the restitution portrait, which we describe in Section 1.2 below.

Many other protocols have been used: see for example<sup>3</sup> (Gilmour et al., 1997; Koller et al., 1998; Kobayashi et al., 1992; Fenton et al., 2002; Fox et al., 2002d).

### 1.2. The restitution portrait

Figure 2a shows the restitution portrait obtained from a small piece of paced bullfrog myocardium, in an experiment where only 1:1 responses were observed. The

<sup>3</sup>This list includes protocols in which APD is measured during fibrillation, which can occur only in spatially extended tissue. By contrast, the present paper is concerned with experiments on a piece of myocardium that is deliberately made small in order to eliminate spatial effects.

dynamic restitution curve forms the “backbone” of the figure. This curve connects all the data points collected in the dynamic protocol, each a steady response of the tissue at a different value of  $B$ . For each data point on the dynamic restitution curve, the restitution portrait also shows (i) a segment of the S1–S2 restitution curve in a neighborhood of the corresponding steady state  $(D_{ss}, A_{ss})$  (these are the “ribs” in the figure) and (ii) pairs  $(D_n, A_{n+1})$  in the transient leading to the steady state (these appear as sequences of dots). In this paper, we fit the data shown in Fig. 2a with a quantitative model.

The restitution portrait shown in Fig. 2a, like others in Kalb et al. (2004), exhibits rate-dependent behavior; specifically:

1. Under rapid pacing but still exhibiting a 1:1 response, the dynamic restitution curve is quite steep, having slope up to 3 or more, while the S1–S2 restitution curves are rather shallow, having slopes on the order of 0.5 or less.
2. The approach to steady state (sometimes called accommodation) is very slow, with a time constant<sup>4</sup> on the order of 20–30 s. Neglecting the first few action potentials, the approach is monotonic and occurs along a straight line with a slope of  $-45^\circ$ . This behavior is observed over the entire range of pacing intervals. (See Fig. 3 below for an illustration of this behavior in the mapping model.)

### 1.3. Mapping models

Although the introduction of 1D mapping models by Nolasco and Dahlen (1968) was a decisive advance in our understanding of restitution, a model of the form (1) cannot exhibit Behaviors 1 or 2. Indeed, for a mapping of this form, dynamic restitution, S1–S2 restitution, and the approach to steady state all fall on the *same* curve, the graph of the function  $G$ .

In an effort to model rate dependence, various authors (Chialvo et al., 1990; Otani et al., 1997; Fox et al., 2002a) have introduced ad hoc 2D mapping models, one variable being  $A_n$  and the other a “memory” variable. It was shown in Kalb et al. (2004) that, although these models exhibit the right qualitative behavior, *no single set of parameter values can match all the data in the restitution portrait, such as in Fig. 2a.* (See Section 3.2 for a summary of the argument.)

In this paper, we introduce a new 2D map that

- admits a choice of parameters that fits all the dynamic restitution data, all the S1–S2 restitution data, and most of the transient data from the restitution portrait in Fig. 2a. (Fig. 2b shows the restitution portrait generated by this map.)

Moreover, as discussed in the Appendix,

- the map can be derived with asymptotic analysis from an idealized ionic model in which memory is associated with the accumulation over time of ions in the cell.

<sup>4</sup>If  $A_n$  tends to  $A_\infty$  as  $n \rightarrow \infty$ , the time constant is defined as

$$B \lim_{n \rightarrow \infty} \frac{A_{n+1} - A_\infty}{A_n - A_\infty}.$$

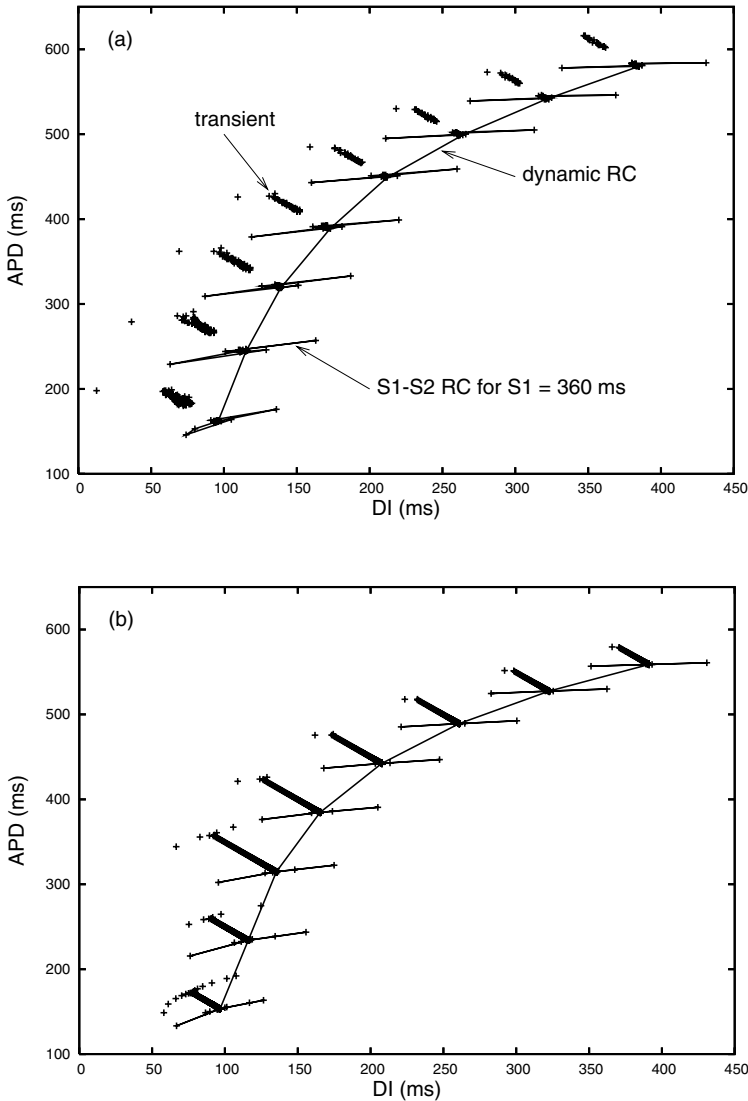


**Fig. 2** (a) The restitution portrait from one of the experiments in Kalb et al. (2004). Remark: Data from late in the transients is not recorded and hence is not shown. (b) The restitution portrait obtained from simulation using the mapping (2, 3) with the parameters in Table 1.

Like the models described in Chialvo et al. (1990), Otani et al. (1997), and Fox et al. (2002a), our mapping contains two variables—one is  $A_n$  as above; the other, which will be denoted by  $C_n$ , specifies an ion concentration in the cell in the underlying ionic model at the start of the  $n$ th action potential (see the Appendix). Under periodic stimulation (say with period  $B$ ), these two variables evolve

according to the iteration<sup>5</sup>

$$A_{n+1} = G(D_n) + \Phi(C_{n+1}) \quad (2)$$

$$C_{n+1} = (C_n + \epsilon)e^{-B/\tau_{\text{pump}}}, \quad (3)$$

where

$$G(D) = A_{\text{max}} + \tau_{\text{fclose}} \ln \{1 - \alpha e^{-D/\tau_{\text{open}}}\} \quad (4)$$

and

$$\Phi(C) = \tau_{\text{sfclose}} \ln \left\{ \frac{\beta e^{-C} + 1}{\beta + 1} \right\}. \quad (5)$$

In (2)–(5),  $A_{\text{max}}$ ,  $\tau_{\text{fclose}}$ ,  $\tau_{\text{sfclose}}$ ,  $\tau_{\text{open}}$ , and  $\tau_{\text{pump}}$  are parameters with the dimensions of time, while  $\epsilon$ ,  $\alpha$ , and  $\beta$  are dimensionless. Note that  $A_{\text{max}}$  is the longest possible APD since in (4) and (5), the terms

$$\tau_{\text{fclose}} \ln \{1 - \alpha e^{-D/\tau_{\text{open}}}\}, \quad \tau_{\text{sfclose}} \ln \left\{ \frac{\beta e^{-C} + 1}{\beta + 1} \right\}$$

are nonpositive and tend to zero under repeated slow pacing.

As we discuss in the Appendix, this mapping was derived as an asymptotic limit of an idealized ionic model, which is a system of ordinary differential equations for three variables: the voltage, an inactivation gate for an inward current, and a generalized concentration. The parameters in (4,5) refer to constants in the ionic model. In particular,  $\tau_{\text{fclose}}$ ,  $\tau_{\text{sfclose}}$  define fast and slow time-scales in the closing of the gate;  $\tau_{\text{open}}$ , the time-scale in the opening of the gate; and  $\tau_{\text{pump}}$ , the time-scale in pumping ions out of the cell.

Below it will be assumed that

$$\tau_{\text{fclose}}, \tau_{\text{sfclose}}, \tau_{\text{open}} \ll \tau_{\text{pump}}. \quad (6)$$

Physiologically,  $\tau_{\text{fclose}}$ ,  $\tau_{\text{sfclose}}$ ,  $\tau_{\text{open}}$  are all on the order of, or shorter than, a typical action potential. Thus, according to (6), only a small fraction of the ions in the cell are pumped out over the course of one action potential.

In the map (2, 3), the effect of the concentration variable is illustrated in Fig. 3a and c, which graph  $A_n$  and  $C_n$  as functions of the beat number  $n$ . The first fifty beats show the steady values for these variables following many stimuli at BCL = 750 ms (assuming parameters as given in Table 1). At  $n = 51$ , the BCL is abruptly decreased to 650 ms. This results in an immediate decrease in  $A_n$ , followed by a slow evolution over 250 beats during which  $C_n$  increases and  $A_n$  decreases. Figure 3b and d show blow-ups of the evolution during the first few beats after the change in BCL; note that  $C_n$  changes only slightly over this short time.

<sup>5</sup>Like (1), the iteration must be modified at extremely short DI's. See Section A.4 of the Appendix for discussion of this issue.

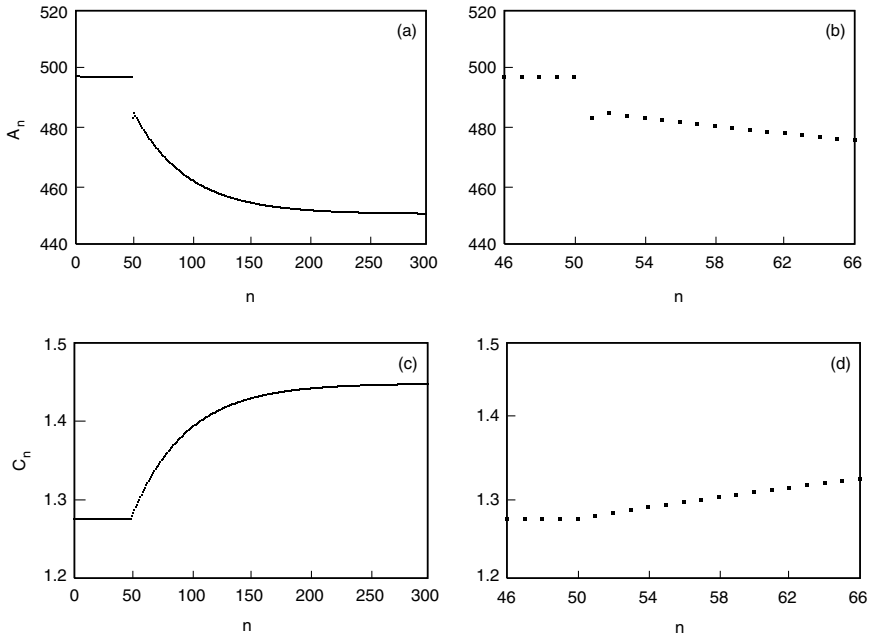


**Fig. 3** (a, c)  $A_n$  and  $C_n$  vs. beat number  $n$ , according to the model (2,3) following an abrupt decrease in BCL from 750 to 650 ms at  $n = 51$ . (Parameter values as in Table 1.) (b, d) The first few beats following the decrease in BCL.

**2. Fitting the mapping to experimental data**

In this section, we choose parameter values in the mapping model (2–5) to best fit the restitution portrait shown in Fig. 2a. Note that the mapping contains eight parameters. One might attempt to determine all these parameters simultaneously with a massive least-squares fit to the entire restitution portrait. However, such a massive fit would not yield any insight about the significance of the individual parameters. Rather, we determine parameters sequentially, in small groups, from four different types of data in the restitution portrait, as follows:

- (1) Slope of the S1–S2 restitution curves at  $S1 = S2$ , where these curves cross the dynamic restitution curve (this slope is denoted  $S_{12}$ ):  $\tau_{open}, \tau_{fclose}, \alpha$
- (2) Slope of the dynamic restitution curve (denoted  $S_{dyn}$ ):  $\tau_{sclose}, \epsilon, \tau_{pump}, \beta$
- (3) Overall height of the dynamic restitution curve:  $A_{max}$ .
- (4) Time constant of the approach to steady state:  $\tau_{pump}$

Table 1 lists parameter values<sup>6</sup> obtained in this way from the data of Fig. 2a.

<sup>6</sup>Of course different parameter values would result from fitting another data set. Incidentally, our model, either the mapping (2, 3) or the underlying ionic model described in the Appendix, is robust—even rather large changes in the parameters do not generally lead to pathological behavior.

### 2.1. $SI-S_2$ restitution data

To determine the slope  $S_{12}$  experimentally, many stimuli (say  $N$ ) are applied with a fixed basic cycle length (say  $B$ ) until the system achieves a steady state, after which the  $(N + 1)$ st stimulus is applied, following a perturbed cycle length  $B + \Delta$ : then  $S_{12}$  is defined by

$$S_{12} = \frac{A_{N+1} - A_N}{D_N - D_{N-1}}. \quad (7)$$

Note that

$$\begin{aligned} A_n &= A_{ss} & \text{for } n \text{ large and } n \leq N, \\ D_n &= D_{ss} & \text{for } n \text{ large and } n < N, \end{aligned}$$

where  $A_{ss}$  and  $D_{ss}$  denote the steady-state values, while

$$D_N = D_{ss} + \Delta, \quad \text{so that} \quad D_N - D_{N-1} = \Delta.$$

If, under the above protocol, a sequence of action potentials is determined by the mapping (2, 3), then the associated concentrations also satisfy

$$C_n = C_{ss} \quad \text{for } n \text{ large and } n \leq N;$$

moreover, since by (6),  $\tau_{\text{pump}}$  is so large,

$$C_{N+1} \approx C_N.$$

Thus, the model (2, 3) predicts that

$$S_{12} \approx G'(D_{ss}). \quad (8)$$

Differentiating (4), we see that the RHS of (8) is given by

$$G'(D_{ss}) = \frac{\tau_{\text{fclose}}}{\tau_{\text{open}}} \frac{\alpha}{e^{D_{ss}/\tau_{\text{open}}} - \alpha}. \quad (9)$$

The squares in Fig. 4a show  $S_{12}$  from the data of Fig. 2a (Kalb et al., 2004). It is natural to try to choose the three parameters in (9),  $\tau_{\text{fclose}}$ ,  $\tau_{\text{open}}$ , and  $\alpha$ , by finding the best fit to these data. However, the quality of the fit is not at all sensitive to  $\tau_{\text{open}}$ , provided this parameter is sufficiently large. This is illustrated in Fig. 4b, which shows the residual as a function of  $\tau_{\text{open}}$  when the corresponding optimal values of  $\tau_{\text{fclose}}$  and  $\alpha$  are chosen. In the remainder of the fitting process we have chosen

$$\tau_{\text{open}} = 500 \text{ ms}. \quad (10)$$

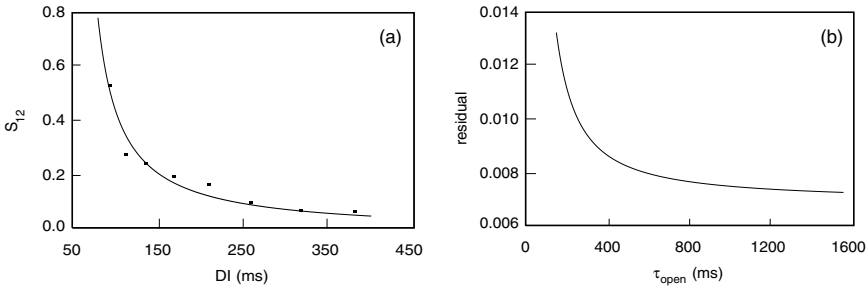


**Fig. 4** (a) A fit of (9) to  $S_{12}$ , the slope of S1–S2 restitution curves. Experimental data is shown by the squares; and the graph of (9) with parameters as in Table 1, by the solid curve. (b) The residual in fitting (9) to  $S_{12}$ , as a function of  $\tau_{open}$ .

(See the discussion in Section A.5(b) of the Appendix concerning the apparent arbitrariness of this choice.) The corresponding optimal values for  $\tau_{fclose}$  and  $\alpha$ , rounded to two significant figures, are given in Table 1. For these values, it is seen in Fig. 4a that the fit of the  $S_{12}$  data from the experiment is very good.

2.2. Slope of the dynamic restitution curve

According to (2), the steady-state action potential duration is given by

$$A_{ss} = G(D_{ss}) + \Phi(C_{ss}). \tag{11}$$

In the physiological range,  $B$  is on the order of a typical action potential duration. The order of magnitude of the action potential duration in the model is determined by the gate time constants  $\tau_{fclose}$ ,  $\tau_{sclose}$ . But by (6), the gate time constants are much smaller than  $\tau_{pump}$ . Thus, we conclude that, in the physiological range,

$$B \ll \tau_{pump}. \tag{12}$$

**Table 1** Parameter values used in the model (2–5) to reproduce the experimental data of Fig. 2(a).

Parameter	Value
$\tau_{open}$ (ms)	500
$\tau_{fclose}$ (ms)	22
$\alpha$	1.1
$\tau_{sclose}$ (ms)	320
$\epsilon \tau_{pump}$ (ms)	980
$\beta$	7.3
$\tau_{pump}$ (ms)	30,000
$A_{max}$ (ms)	840

Given (12), it follows from expanding the exponential in (3) that

$$C_{ss} \approx \Phi(\epsilon \tau_{\text{pump}}/B). \quad (13)$$

Combining (11, 13), we find that

$$A_{ss} \approx G(D_{ss}) + \Phi(\epsilon \tau_{\text{pump}}/B). \quad (14)$$

Since  $B = A_{ss} + D_{ss}$ , (14) defines  $A_{ss}$  implicitly as a function of  $D_{ss}$ , and (14) may be differentiated to yield the slope of the dynamic restitution curve

$$S_{\text{dyn}} = \frac{dA_{ss}}{dD_{ss}} \approx G'(D_{ss}) - \frac{d\Phi}{dC} \frac{\epsilon \tau_{\text{pump}}}{B^2} (S_{\text{dyn}} + 1), \quad (15)$$

where we have used the fact that  $dB/dD_{ss} = S_{\text{dyn}} + 1$ . Recalling (8), computing  $d\Phi/dC$  from (5), and rearranging, we obtain

$$\frac{S_{\text{dyn}} - S_{12}}{S_{\text{dyn}} + 1} \approx \frac{\tau_{\text{sclose}} \epsilon \tau_{\text{pump}}}{B^2} \frac{\beta}{\beta + e^{\epsilon \tau_{\text{pump}}/B}}. \quad (16)$$

Note that by forming the combination of slopes on the LHS of (16), we have eliminated the parameters  $\tau_{\text{open}}$ ,  $\tau_{\text{fclose}}$ , and  $\alpha$  from the RHS of (16). Thus, the fitting of (16) is not affected by the nonuniqueness of  $\tau_{\text{open}}$  at the previous stage.

The squares in Fig. 5a show the combination of the slopes  $S_{\text{dyn}}$  and  $S_{12}$  on the LHS of (16) computed from the data<sup>7</sup> of Fig. 2a (Kalb et al., 2004). The curve in the figure<sup>8</sup> shows the fit to these data with  $\tau_{\text{sclose}}$  chosen to be 320 ms and the best corresponding values for  $\epsilon \tau_{\text{pump}}$ ,  $\beta$ , which are given in Table 1. As shown in Fig. 5b, the quality of the fit<sup>9</sup> is not very sensitive to  $\tau_{\text{sclose}}$ .

### 2.3. The two remaining parameters

The parameter  $A_{\text{max}}$  sets the overall height of the dynamic restitution curve. The fit of the model (2, 3) with  $A_{\text{max}} = 840$  ms to the dynamic restitution curve from Kalb et al. (2004) is shown in Fig. 6.

Steady-state data determine the product  $\epsilon \tau_{\text{pump}}$  but neither factor individually; for the individual factors, we turn to the transient data. In the perturbed down-sweep protocol (Kalb et al., 2004), each time the basic cycle length is decreased, a

<sup>7</sup>More accurately, data for  $S_{\text{dyn}}$  were taken from the experiment, but values for  $S_{12}$  from our fit of (9) were used.

<sup>8</sup>Of the various parameter fits in the paper, Fig. 5a is perhaps the least satisfactory. Note that this weakness is far less clear in the fit of Fig. 6, an integrated version of (16). This difference illustrates the point that data from the restitution portrait provide a demanding test of any mathematical model.

<sup>9</sup>In fact, as may be seen from the figure, the residual is not minimized by the value for  $\tau_{\text{sclose}}$  that we have chosen. The value  $\tau_{\text{sclose}} = 320$  ms is a compromise: we accept a residual that is 15% larger than the minimum in order to reduce the error in the leading-order asymptotics used in deriving the mapping from the idealized ionic model. (See Schaeffer et al. (2006).)

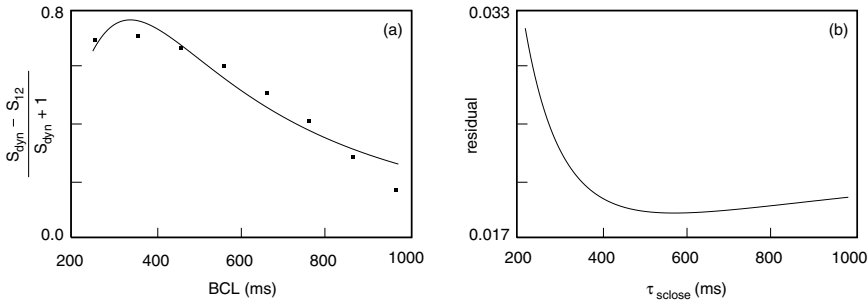


**Fig. 5** (a) A fit of (16) to data involving  $S_{\text{dyn}}$ , the dynamic restitution slope. (b) The residual in fitting (16) to these data, as a function of  $\tau_{\text{sclose}}$ .

time constant is extracted from the transient to the next steady state. These time constants are typically on the order of 20–30 s, decreasing somewhat as  $B$  is decreased (see Fig. 4 of Elharrar and Surawicz (1983) or Kalb et al. (2004)). In the mapping model (2, 3), the time constant of such transients is very nearly equal to  $\tau_{\text{pump}}$ , for all  $B$ . As indicated in Table 1, we assume a constant<sup>10</sup>  $\tau_{\text{pump}} = 30,000$  ms, which yields  $\epsilon = 0.033$ .

### 3. Discussion of the mapping, including its limitations

#### 3.1. Comparison with previous mathematical models

It is instructive to compare our model to the ad hoc models of Chialvo et al. (1990) and Fox et al. (2002a), in which the action potential duration  $A_n$  and the memory variable  $M_n$  evolve according to

$$A_{n+1} = (1 - \alpha M_{n+1})G(D_n) \tag{17a}$$

$$M_{n+1} = \{1 - (1 - M_n)e^{-A_n/\tau}\} e^{-D_n/\tau}. \tag{17b}$$

Even though Eq. (17b) differs only subtly from (3), no single set of parameters in a model of the form (17) fits all the data in Fig. 2a. The complete discussion of this point in Kalb et al. (2004) is too long to reproduce here, but the following is the crux of the argument:

We claim that (17), combined with parts of the data of Fig. 2a, leads to the prediction that, for small DI, one has  $S_{\text{dyn}} < S_{12}$ . This condition was never observed in the experiments of Kalb et al. (2004). To see why (17) makes this prediction contrary to experiment, observe that, in order to have long transients following a decrease in the BCL, the parameter  $\tau$  in (17b) must be large. Now let  $A_{\text{ss}}, D_{\text{ss}}$ ,

<sup>10</sup>Equation (3) derives from the ionic model in the Appendix: specifically, (A.13) describes a linear pump that pumps at a very slow, constant rate. The ionic model could easily be modified to follow the experiments more closely.

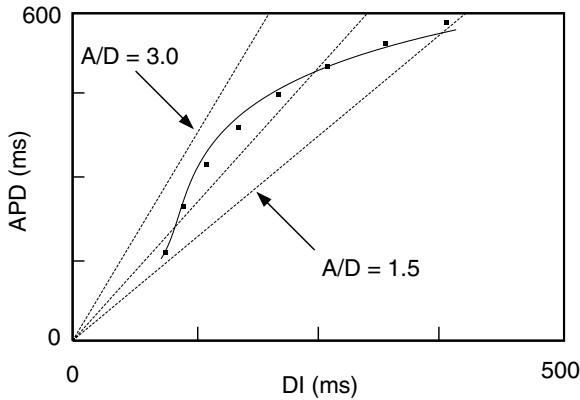


**Fig. 6** The solid line shows a fit of (2, 3) to the dynamic restitution curve. Also shown are three dashed lines along which the ratio  $A/D$  is constant (specifically,  $A/D = 1.5, 2, 3$ ), which will facilitate the discussion in Section 3.1.

and  $M_{ss}$  be the steady-state values of these variables under iteration of (17), as a function of the basic cycle length  $B$ . Since  $\tau$  is large, we may argue as in (8, 15) that

$$S_{12} \approx (1 - \alpha M_{ss})G'(D_{ss})$$

and

$$S_{dyn} \approx S_{12} - \alpha G(D_{ss}) \frac{dM_{ss}}{dD_{ss}}. \tag{18}$$

Expanding the exponentials in (17b), we obtain

$$M_{ss} \approx \frac{A_{ss}}{A_{ss} + D_{ss}}.$$

Note that  $M_{ss}$  is a monotone increasing function of the ratio  $A_{ss}/D_{ss}$ . It may be seen from the lines of constant  $A_{ss}/D_{ss}$  in Fig. 6 that, for small DI, the ratio  $A_{ss}/D_{ss}$  decreases if the DI decreases. Therefore,  $dM_{ss}/dD_{ss} > 0$ . On substitution into (18), we obtain, for small DI, the prediction that  $S_{dyn} < S_{12}$ , as claimed.

In contrast to (17), for the mapping (2–5), the steady-state value of  $C$  is given by (13), so the derivative  $dC_{ss}/dD_{ss}$  is *negative* for *all* values of the DI. Thus,  $S_{12} < S_{dyn}$ .

Regarding the origin of this difference between mappings, (13) derives from (3), which may be traced to an assumption in the idealized ionic model discussed in the Appendix: i.e., as stated in (A.13, A.14),

a fixed charge  $\epsilon$  enters the cell during the upstroke of each action potential and charge is pumped out at a constant rate throughout BCL.

As shown in [Otani et al. \(1997\)](#), evolution similar to (17b) could also be obtained from an ionic model: specifically, a model in which

charge accumulates in the cell during the action potential and is pumped out during the diastolic interval.

Thus, having an ionic basis for the mapping, even an unrealistically simple one, clarifies how the present model differs from previous models.

Another difference between models is that the memory effect in (2) is *additive*, while it is multiplicative in (17). This difference may be traced to the logarithmic dependence in the restitution function (A.6) derived from the ionic model.

### 3.2. Comparison with the experiments of Elharrar and Surawicz

[Elharrar and Surawicz \(1983\)](#) parametrize the dependence of the steady-state action potential  $A_{ss}$  on the period  $B$  with a function that has the asymptotic form as  $B \rightarrow \infty$

$$A_{ss} \sim A_{\max} - \text{Const}/B. \quad (19)$$

This algebraic decay matches the experimental observation ([Elharrar and Surawicz, 1983](#)) that  $A_{ss}$  continues to increase significantly as  $B$  is raised beyond physiological values. Let us show that the present model (2, 3) exhibits such algebraic decay for large  $B$ . By (4), the function  $G(D)$  will contribute a constant term to (19) but no term at the level  $\mathcal{O}(1/B)$ . Recalling that (12) holds in the physiological range and referring to (4, 5), we obtain (19) on substitution into (11), where the coefficient of  $1/B$  equals

$$\frac{\beta}{\beta + 1} \tau_{\text{sclose}} \in \tau_{\text{pump}}.$$

In a different direction, the experiments of [Elharrar and Surawicz](#) measured what might be called *global* S1–S2 restitution curves: i.e., the graph of action potential duration as a function of S2, when S2 varies over its entire range (with S1 fixed). By contrast, the restitution portrait from [Kalb et al. \(2004\)](#) shows only *local* S1–S2 restitution: i.e., only perturbed intervals S2 nearly equal to S1 are explored. Of course global restitution provides more data to test a model, and experiments are planned to test the predictions of the model (2, 3) in this regard.

One successful qualitative prediction of the present model (2, 3) regarding global S1–S2 restitution may already be reported. [Elharrar and Surawicz \(1983\)](#) found that each S1–S2 curve crosses the dynamic restitution curve twice, first for  $S2 = S1$  and then again for small DI. Observe that  $G(D)$  given by (4) tends to negative infinity<sup>11</sup> as  $D$  tends to  $D_{\text{sing}} = \tau_{\text{open}} \ln \alpha > 0$  from above. Thus, the S1–S2 and dynamic restitution curves produced by using this formula for all DI's also intersect twice in this way.

---

<sup>11</sup>Even though, as discussed in the Appendix, the formula (4) is modified at small DI's before the singularity at  $D_{\text{sing}}$  is reached, the conclusion about two intersections remains valid.

### 3.3. Another form for memory

In Kalb (2004) or Tolkacheva et al. (2004), memory is introduced into restitution by a mapping of the form

$$A_{n+1} = \Psi(A_n, D_n, D_{n-1}). \quad (20)$$

Let us show that (2–5) can be recast in this form. Note that the function  $\Phi(C)$  in (5) is monotonic in  $C$ , so that it has an inverse function. From (2) at the previous iterate we deduce that

$$C_n = \Phi^{-1}(A_n - G(D_{n-1})).$$

Substituting into (2, 3) we obtain (20), where

$$\Psi(A_n, D_n, D_{n-1}) = G(D_n) + \Phi \left( [\Phi^{-1}(A_n - G(D_{n-1})) + \epsilon] e^{-(A_n + D_n)/\tau_{\text{pump}}} \right).$$

Although this alternative form is available, we believe that (2–5) offers greater clarity, in part because processes at different time scales are separated by appearing in different equations.

### 3.4. Limitations and future work

The present model fits the experiments of Kalb et al. (2004) remarkably well, especially considering the simplicity of the model. However, at very rapid pacing some differences between the model and experiment become apparent. For example, in Fig. 2 consider the transient following the jump to the shortest BCL. In the experiment, after one very short DI, there is almost no oscillation in the remainder of the transient. By contrast, in the mapping, oscillations die out only after approximately a dozen stimuli. Moreover, in the figure the transient shown for the mapping is shorter than for the experiment because of another difference between experiment and model. In the experiment, BCL was decremented in steps of approximately 100 ms. In computations with the mapping, at the two shortest BCL's, steps this large led to initial diastolic intervals so short that the approximations behind the derivation of the mapping fail (see Section A.4 of the Appendix). When this difficulty arose, the decrease in BCL was performed in two smaller steps, and Fig. 2b shows only the transient from the last decrease of BCL.

The present model is based on experiments with exclusively a 1:1 response. At least in its present form, it is unable to predict the onset of alternans. Mathematically, alternans begins when an eigenvalue of the differential of the mapping passes through  $-1$ . For the present mapping, one of its two eigenvalues is close to  $+1$  (on the order of  $e^{-B/\tau_{\text{pump}}}$ ), and the other is approximately  $-S_{12}$ . In the experiments of Kalb et al. (2004), if alternans were observed, then typically  $S_{12}$  was about  $1/2$ . Thus, the condition  $\lambda = -1$  cannot be satisfied by either eigenvalue of the mapping. In mammals, the cycling of Ca between the sarcoplasmic

reticulum and the cytosol might be the extra ingredient needed to model alternans successfully. In frogs, however, the exchange of Ca between the sarcoplasmic reticulum and the cytosol is muted or absent, and the situation is far less clear (Morad and Cleemann, 1987).

Although we have modeled memory through a generalized ionic concentration  $C$ , we cannot associate a specific ion (or combination of ions) with this variable. It could, for example, represent either sodium or calcium, both of which are known to build up slowly in the cardiac cell during rapid pacing (see Section A.5 in the Appendix), similar to the behavior of  $C$  in our model, as illustrated in Fig. 3. Moreover, even if  $C$  is associated with calcium, our model does not attempt to describe the rapid exchange of calcium between the sarcoplasmic reticulum and the cytosol, such as occurs at least in mammalian hearts (Bassani et al., 1995). On the contrary, the concentration  $C$  would correspond to the *total* concentration of calcium in the cell, which evolves on a much slower time scale than the concentration in either the sarcoplasmic reticulum or the cytosol individually (cf. Shiferaw et al., 2003).

It may seem like a limitation of the model that, as a mapping, it can characterize the dynamics of APD's only at one site. However, this limitation is only apparent. Because the mapping is derived as an asymptotic limit of an ionic model (see the Appendix), given parameter values for the mapping, we can substitute these into (A.7, A.11, A.13) and obtain a system of ODE's with equivalent behavior. This system of ODE's can readily be extended to obtain a PDE model, which can then be used to study electrotonic effects and propagation.

In the longer term, we seek to automate the calculations of Section 2 in which the parameters of the mapping are fit to experimental data. Our goal is to be able to obtain a mathematical model of a given animal's response *while the tissue is still alive*. This will allow us to test the predictive, as well as the descriptive, capacity of the mapping. Such a rapid fitting to experiment is more feasible with a mapping model than with an ionic model. Moreover, since the present mapping is derived as an asymptotic limit of an idealized ionic model, we may use this ionic basis to overcome some of the limitations of mapping models.

#### 4. Conclusions

In this paper, we have made the following points. The Appendix elaborates on the third and fourth items.

- Complex, rate dependent restitution, including memory, can be modeled remarkably well by the simple 2D mapping (2, 3). (See Figs. 2, 4a, and 5a.)
- Because of the simplicity of the fitting procedure, one may choose parameters in (2, 3) to fit restitution portraits from other experiments or from physiologically detailed ionic models. In particular, in Kalb et al. (2004) the mapping was fitted to the ionic model of Fox et al. (2002c).
- The mapping is derived from an idealized ionic model, in which memory occurs through the accumulation of charge in the cell. The assumptions needed to fit the model to data (e.g., (A.14) provide partial information about which currents in realistic models may contribute to rate dependence.

- Matching restitution data is insufficient validation of an ionic model: even in the present, greatly simplified model, very different choices of some of the parameters can fit the data equally well.

## Acknowledgements

The Support of the National Institutes of Health under grant 1R01-HL-72831 and the National Science Foundation under grants PHY-0243584 and DMS-9983320 is gratefully acknowledged.

## Appendix A: Ionic basis of the mapping

### A.1 A two-current idealized ionic model

The present work builds on the two-current ionic model of Karma (1993) and of Mitchell and Schaeffer (2003), which we now summarize. The two-current model contains two functions of time, the transmembrane potential  $v(t)$  and a gating variable  $h(t)$ , both of which are dimensionless and scaled to lie in the interval  $(0, 1)$ . They satisfy the following ordinary differential equations:

$$\frac{dv}{dt} = -J_{\text{in}}(v, h) - J_{\text{out}}(v), \quad (\text{A.1})$$

and

$$\frac{dh}{dt} = \begin{cases} (1-h)/\tau_{\text{open}} & \text{if } v \leq v_{\text{crit}}, \\ -h/\tau_{\text{close}} & \text{if } v > v_{\text{crit}}. \end{cases} \quad (\text{A.2})$$

The outward current in (A.1) is linear in  $v$ ,

$$J_{\text{out}}(v) = \frac{v}{\tau_{\text{out}}}, \quad (\text{A.3})$$

and the inward current is given by

$$J_{\text{in}}(v, h) = -\frac{h}{\tau_{\text{in}}}\phi(v), \quad (\text{A.4})$$

where the voltage dependence is cubic:  $\phi(v) = v^2(1-v)$ . The constants  $\tau_{\text{in}}$ ,  $\tau_{\text{out}}$ ,  $\tau_{\text{open}}$  and  $\tau_{\text{close}}$  set the time scales for the four phases of an action potential; specifically, the duration of the upstroke, plateau, repolarization, and rest phases are set by  $\tau_{\text{in}}$ ,  $\tau_{\text{close}}$ ,  $\tau_{\text{out}}$  and  $\tau_{\text{open}}$ , respectively. In Mitchell and Schaeffer (2003), based on the assumption that

$$\tau_{\text{in}} \ll \tau_{\text{out}} \ll \tau_{\text{open}}, \tau_{\text{close}},$$

an explicit leading-order asymptotic approximation<sup>12</sup> for the restitution curve is derived from the two-current model: specifically

$$A_{n+1} \approx F(D_n), \tag{A.5}$$

where

$$F(D) = \tau_{\text{close}} \ln \left\{ \frac{1 - (1 - h_{\text{min}})e^{-D/\tau_{\text{open}}}}{h_{\text{min}}} \right\} \tag{A.6}$$

and  $h_{\text{min}} = 4\tau_{\text{in}}/\tau_{\text{out}}$ . Note that this model does not exhibit any rate dependence.

### A.2 The ionic model including concentration

We augment the two-current model (A.1, A.2) by adding a third variable, a generalized concentration  $c$ , and modifying the equations as follows:

- (i) The new equation for the transmembrane potential reads

$$\frac{dv}{dt} = -J_{\text{in}}(v, h, c) - J_{\text{out}}(v), \tag{A.7}$$

where the outward current is still given by (A.3), but the inward current is now the sum of *concentration-independent* ( $\phi_{\text{ci}}$ ) and *concentration-dependent* ( $\phi_{\text{cd}}$ ) parts

$$J_{\text{in}}(v, h, c) = -\frac{hv}{\tau_{\text{in}}} \{ \phi_{\text{ci}}(v) + \beta e^{-c} \phi_{\text{cd}}(v) \}, \tag{A.8}$$

with  $\beta$  a constant. It may be seen from (A.8) that the build-up of charge in the cell weakens the inward current, thereby shortening action potentials. The behavior of the model is not very sensitive to the exact form of the functions  $\phi_{\text{ci}}(v)$  and  $\phi_{\text{cd}}(v)$ . To simplify the derivation via asymptotics of the 2D mapping model from the ionic model (see Schaeffer et al. (2006)), we set these functions equal to piecewise linear functions of  $v$ , as follows:

$$\phi_{\text{ci}}(v) = \begin{cases} \frac{v}{v_{\text{crit}}} & \text{if } v \leq v_{\text{crit}}, \\ 1 & \text{if } v_{\text{crit}} < v \leq 1 - v_{\text{crit}}, \\ \frac{1-v}{v_{\text{crit}}} & \text{if } 1 - v_{\text{crit}} < v. \end{cases} \tag{A.9}$$

and

---

<sup>12</sup>The first correction to (A.6) is derived in Cain and Schaeffer (2006). This correction significantly improves the accuracy of the approximation.

$$\phi_{cd}(v) = \begin{cases} 0 & \text{if } v \leq v_{crit}, \\ 1 - \frac{|1-2v|}{1-2v_{crit}} & \text{if } v_{crit} < v \leq 1 - v_{crit}, \\ 0 & \text{if } 1 - v_{crit} < v. \end{cases} \tag{A.10}$$

(ii) The Eq. (A.2) for the gating variable  $h$  is modified by assuming that the gate closes at a voltage-dependent rate,

$$\frac{dh}{dt} = \begin{cases} (1 - h)/\tau_{open} & \text{if } v \leq v_{crit}, \\ -h/T_{close}(v) & \text{if } v > v_{crit}. \end{cases} \tag{A.11}$$

Specifically, the closing rate is taken as piecewise linear in  $v$ ,

$$\frac{1}{T_{close}(v)} = \begin{cases} \frac{1}{\tau_{fclose}} - \left(\frac{1}{\tau_{fclose}} - \frac{1}{\tau_{sclose}}\right) \frac{1-v}{1-v_{sldn}} & \text{if } v > v_{sldn}, \\ \frac{1}{\tau_{sclose}} & \text{if } v \leq v_{sldn}. \end{cases} \tag{A.12}$$

Note that two different time-scale parameters,  $\tau_{fclose}$  and  $\tau_{sclose}$ , derive from the closing of the gate. (Remark: The subscript *sldn* is mnemonic for “slow down.”)

(iii) The concentration is determined by a balance between  $I(t)$ , the current which leads to the build-up of charge in the cell, and constant linear pumping, which removes charge from the cell<sup>13</sup>:

$$\frac{dc}{dt} = -I(t) - \frac{c}{\tau_{pump}}. \tag{A.13}$$

The current  $I(t)$  should satisfy two key properties:

- $I(t)$  is nonzero only during the upstroke of an action potential, and
- A fixed charge  $\epsilon$  enters the cell during the upstroke of each action potential: in symbols,

$$\int_{t_{stim}}^{t_{stim}+B} I(t)dt \approx -\epsilon. \tag{A.14}$$

The precise form of  $I(t)$  is not important; to achieve the properties above we choose

$$I(t) = \begin{cases} \frac{\epsilon}{1-v_{crit}} (J_{in} + J_{out}) & \text{if } v > v_{crit} \quad \text{and} \quad \frac{dv}{dt} > 0, \\ 0 & \text{otherwise.} \end{cases} \tag{A.15}$$

---

<sup>13</sup>Although Eq. (A.13) appears to be nonautonomous, the expression (A.15) may be seen to yield an autonomous equation. However, since  $I(t)$  is a function of  $dv/dt$  as well as  $v$  itself, we prefer the notation in (A.13).

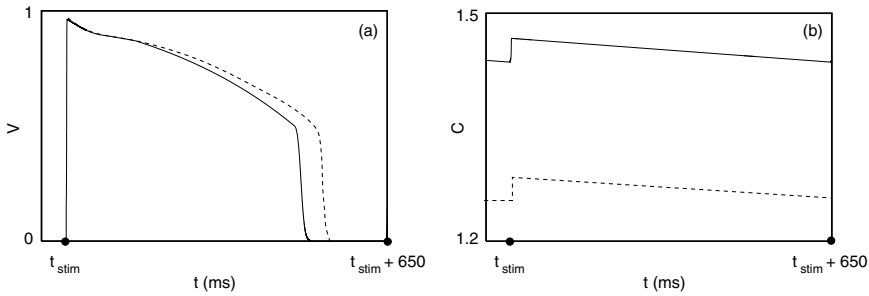


**Fig. 7** Voltage and concentration vs. time in the ionic model (A.7), (A.11) and (A.13) with the parameter values in Table A.1. *Solid line:* steady state response at  $B = 650$  ms. *Dashed line:* First response at  $B = 650$  ms, following steady state at  $B = 750$  ms.

The Eqs. (A.7), (A.11) and (A.13) define the three-variable idealized ionic model. Figure 7 shows two time traces of the voltage and concentration at a basic cycle length  $B = 650$  ms. (Model parameters are chosen as in Table A.1. The gate variable  $h$  is not plotted since it is less interesting.) The solid curve represents the steady-state response following many stimuli at this basic cycle length, while the dashed curve represents the response to the *first* stimulus with  $B = 650$  ms, following many stimuli at  $B = 750$  ms. Note that at steady state, the concentration has built up to larger values, resulting in shorter action potentials. On the order of 200 beats are required for the concentration to build up to its steady state. Figure 3c shows this gradual build up of concentration for the mapping model (2, 3) that approximately describes the behavior of the ionic model,<sup>14</sup> as we now discuss.

### A.3 Approximation of the ionic model by a mapping

Under the assumption that

$$\tau_{in} \ll \tau_{out} \ll \tau_{open}, \tau_{fclose}, \tau_{sclose} \ll \tau_{pump}, \tag{A.16}$$

a 2D mapping can be extracted<sup>15</sup> as an asymptotic limit of (A.7), (A.11) and (A.13). Specifically, let  $A_n$  be the duration of the  $n$ th action potential and  $C_n$  the ionic concentration at the start of the  $n$ th action potential. It is shown in Schaeffer et al. (2006) that, under periodic stimulation at all but the highest pacing rates, the two variables  $A_n$  and  $C_n$  evolve approximately according to the iteration (2, 3). These formulas represent the leading order in an asymptotic expansion in the parameter  $\tau_{out}/\tau_{sclose}$ .

<sup>14</sup>Incidentally, the APD's in Fig. 7 are on the order of 5% longer than the values graphed in Fig. 3. This discrepancy provides an estimate for the degree of accuracy of the asymptotic approximation. As in Cain and Schaeffer (2006), inclusion of the first correction to the leading order significantly improves the approximation.

<sup>15</sup>For the derivation of (2–5), it is also assumed that  $v_{crit} \geq 1 - v_{sldn}$ . The case where this inequality is reversed may be analyzed similarly.

**Table A.1** Parameter values for the ionic model (A.7), (A.11), (A.13).

Parameter	Value
$\tau_{in}$ (ms)	0.28
$\tau_{out}$ (ms)	3.2
$\beta$	7.3
$v_{crit}$	0.13
$v_{sldn}$	0.89
$\tau_{open}$ (ms)	500
$\tau_{fclose}$ (ms)	22
$\tau_{sclose}$ (ms)	320
$\tau_{pump}$ (ms)	30,000
$\epsilon$	0.033

Note that the restitution function in (4) contains two parameters,  $\alpha$  and  $A_{max}$ , that do not appear in the ionic model (A.7), (A.11), (A.13); these are given by

$$\alpha = \left\{ 1 - \frac{\tau_{in}}{\tau_{out}} \left( 1 - \frac{\tau_{fclose}}{\tau_{sclose}} \right) \frac{v_{crit}}{1 - v_{sldn}} \right\}^{-1} \quad (\text{A.17})$$

and

$$A_{max} = \tau_{fclose} \ln \left\{ \frac{\tau_{sclose}}{\tau_{fclose}} \frac{\tau_{out}}{\tau_{in}} \frac{1}{\alpha} \frac{(1 - v_{sldn})}{v_{crit}} \right\} + \tau_{sclose} \ln \left\{ (\beta + 1) \frac{v_{crit}}{1 - v_{sldn}} \right\}. \quad (\text{A.18})$$

The parameter values in Table A.1, with substitution into (A.17) and (A.18), yield the parameters for the mapping that are given in Table 1, to within round-off errors.

#### A.4 Modifications at extremely rapid pacing

In all mapping models for cardiac restitution, special considerations must be invoked at extremely rapid pacing. For example, with the Nolasco–Dahlen (1968) model

$$A_{n+1} = G(D_n), \quad (\text{A.19})$$

usually one posits a minimum diastolic interval, say  $D_{thr}$ , such that (A.19) holds only if  $D_n > D_{thr}$ . For the map (A.6), which is derived from the ODE's (A.1) and (A.2), it is shown in Mitchell and Schaeffer (2003) that this threshold behavior follows from asymptotic analysis of the underlying ionic model. Specifically, suppose the stimulus current raises the voltage by an amount  $v_{stim}$  in a time that is short compared to  $\tau_{in}$ ; then the threshold DI for (A.6) is given by

$$D_{thr} = \tau_{open} \ln \left( \frac{1 - h_{min}}{1 - h_{stim}} \right) \quad \text{where} \quad h_{stim} = \frac{\tau_{in}/\tau_{out}}{v_{stim}(1 - v_{stim})}.$$

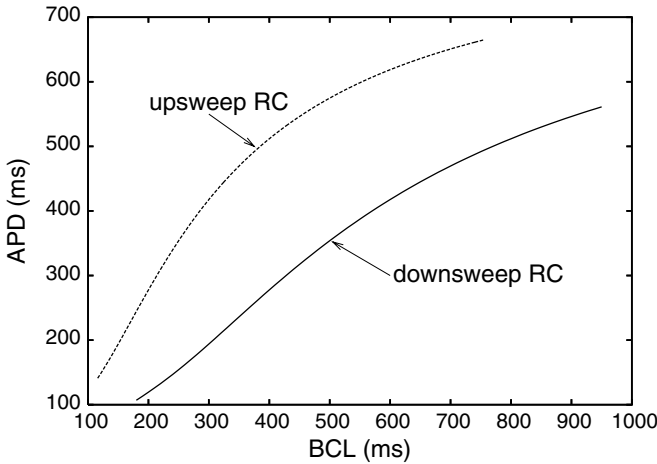


**Fig. 8** The restitution curve from the mapping showing 2:1 steady-state behavior (*dashed curve*) as well as 1:1 behavior (*solid curve*). Parameters as in Table 1, with  $D_{thr} = 80$  ms.

If  $D_n < D_{thr}$ , the heart is assumed to ignore the stimulus and wait for a later stimulus. (For the mapping (A.6), this behavior is derived from asymptotics in Mitchell and Schaeffer (2003).) Thus, if the heart is paced at a constant, very short, basic cycle length  $B$ , the effective diastolic interval is  $kB - A_n$ , where

$$k \text{ is the smallest integer such that } kB - A_n > D_{thr}. \tag{A.20}$$

For mathematical completeness, the iteration (A.19) should therefore be written

$$A_{n+1} = G(kB - A_n) \tag{A.21}$$

with  $k$  given by (A.20). Using this formula one can obtain, at sufficiently short BCL, 2:1, 3:1, etc. responses from a simple one-dimensional mapping. In the experiment summarized in Fig. 2a, when BCL became too small the sample jumped to a 2:1 rhythm, and such higher-order rhythms were not investigated.

Similarly, the present 2D mapping needs to be modified at extremely rapid pacing. These modifications may be derived from the underlying ionic model. The full analysis, which is presented in Schaeffer et al. (2006), is somewhat technical; here we record only the following points.

- Strictly speaking, the threshold diastolic interval depends on the concentration  $C_n$  (as well as on  $v_{stim}$ ); however, to leading order in the asymptotics  $D_{thr}$  is independent of the concentration, and we make this approximation. If  $D_n < D_{thr}$ , then the formula for  $A_{n+1}$  must be modified analogously to (A.21), which gives

rise to 2:1 and higher-order rhythms. Figure 8 shows steady-state 2:1 responses<sup>16</sup> of the mapping with parameter values as in Table A.1, along with the steady-state 1:1 responses already studied, where we have assumed  $D_{\text{thr}} = 80$  ms. (Note that the shortest steady-state DI in Fig. 2a is 95 ms.)

- For very small DI, but still greater than  $D_{\text{thr}}$ , the assumptions in the derivation of (2, 3, 4, 5) may break down. Let

$$h_{\text{sldn}} = \frac{\tau_{\text{in}}}{\tau_{\text{out}}} \frac{v_{\text{crit}}}{1 - v_{\text{sldn}}}, \quad \text{and} \quad D_{\text{sldn}} = \tau_{\text{open}} \ln \left( \frac{1}{1 - h_{\text{sldn}}} \right).$$

If  $D_n > D_{\text{sldn}}$ , then  $A_{n+1}$  is still given by (2, 4, 5), but if  $D_{\text{thr}}(C_n) < D_n < D_{\text{sldn}}$  then the formula for  $A_{n+1}$  must be changed. (For the parameter values in Table A.1,  $D_{\text{sldn}} = 51$  ms.) This change is not relevant for the parameter fit in Section 2 because all steady-state DI's in Fig. 2 lie above the range where the change is needed.

## A.5 Comments on the model

### A.5.1. Concentration as a memory variable

The use of concentration as a memory variable was motivated by numerical simulations of the restitution portrait using the Luo-Rudy-dynamic (LRd) model (Luo and Rudy, 1994). It is known that a step decrease in the basic cycle length BCL causes a slow and monotone decrease in action potential duration, an increase in concentration of intracellular sodium ( $[\text{Na}^+]_i$ ), and a decrease in concentration of potassium ( $[\text{K}^+]_i$ ); these transients have been seen both in the LRd model (Hund et al., 2001) and in experiments (Cohen et al., 1982). Our simulations of the LRd model show that the decrease of APD is most sensitive to  $[\text{Na}^+]_i$ : specifically, holding  $[\text{Na}^+]_i$  constant greatly shortens the APD transient and eliminates most of the memory features from the restitution portrait (Oliver et al., 2004). Thus, originally we regarded the concentration variable  $c(t)$  as modeling  $[\text{Na}^+]_i$ , and assumption (A.14) on  $I(t)$  was motivated by the behavior of the fast sodium current.

However, other interpretations of  $c(t)$  are possible. For example, in the Fox–McHarg–Gilmour model (Fox et al., 2002c), we have found that memory can be largely eliminated by holding constant the concentration of calcium in the sarcoplasmic reticulum (Kalb et al., 2004). Thus,  $c(t)$  might also be associated with a calcium concentration. In this connection, it is noteworthy that both the L-type calcium current and the release of calcium from the sarcoplasmic reticulum have spikes near the beginning of an action potential (Greenstein and Winslow, 2003; Shiferaw et al., 2003), suggestive of the assumptions on  $I(t)$ . In any case, one should probably be wary of too literal an interpretation of  $c(t)$ .

<sup>16</sup>In the computations of this figure, we assumed that an unsuccessful stimulus had no effect on the concentration variable. In seeking to match experiments including 2:1 behavior, one might want to alter this assumption.

### A.5.2. Consequences of requiring an ionic basis for the mapping

In the nonlinear least-squares fitting of the mapping to data, the quality of the fit was rather insensitive to  $\tau_{\text{open}}$  and  $\tau_{\text{close}}$ . As this fact suggests, the data in the restitution portrait could be fit by a mapping with fewer parameters. For example, the RHS of (9) contains three parameters. If  $\tau_{\text{open}} \rightarrow \infty$  and at the same time  $\alpha \rightarrow 1$  so that the product  $(\alpha - 1)\tau_{\text{open}} \rightarrow D_{\text{sing}}$ , the RHS of (9) reduces to

$$\frac{\tau_{\text{fclose}}}{D_{\text{ss}} - D_{\text{sing}}}. \quad (\text{A.22})$$

This two-parameter form is sufficient to fit the  $S_{12}$ -data of Fig. 4a; indeed, since the residual in Fig. 4b gets smaller as  $\tau_{\text{open}} \rightarrow \infty$ , formula (A.22) fits the data slightly *better* than (9) with the parameter values of Table 1. However, in the ionic model, letting  $\tau_{\text{open}} \rightarrow \infty$  makes no sense, so we have not attempted to eliminate parameters in this way.<sup>17</sup>

Three specific ways in which the ionic basis influenced the form of our mapping are as follows:

- We assumed that the evolution of the gate variable in the ionic model depended only on voltage, not on concentration.
- We allowed distinct values for parameters in the ionic model that were associated with different functions. For example, in fitting the  $S_{\text{dyn}}$ -data in Fig. 5a, one could take  $\tau_{\text{close}} = \epsilon \tau_{\text{pump}}$  without affecting the fit adversely. Although this would eliminate a parameter from the mapping, it seems unnatural to build such an assumption into the ionic model.
- We limited parameters to physiologically reasonable values. For this reason we assumed in (10) that  $\tau_{\text{open}} = 500$  ms, even though larger values led to a slightly smaller residual.

## References

- Banville, I., Gray, R.A., 2002. Effect of action potential duration and conduction velocity restitution and their spatial dispersion on alternans and the stability of arrhythmias. *J. Cardiovasc. Electrophysiol.* 13, 1141–1149.
- Bassani, J., Yuan, M., Bers, D., 1995. Fractional SR Ca release is regulated by trigger Ca and SR Ca content in cardiac myocytes. *Am. J. Physiol.* 268, C1313–C1319.
- Cain, J., Schaeffer, D., 2006. Two-term asymptotic approximation of a cardiac restitution curve. *SIAM Review*, in press.
- Cherry, E.M., Fenton, F.H., 2004. Suppression of alternans and conduction blocks despite steep APD restitution: Electrotonic, memory, and conduction velocity restitution effects. *Am. J. Physiol.* 286, H2332–H2341.
- Chialvo, D.R., Michaels, D.C., Jalife, J., 1990. Supernormal excitability as a mechanism of chaotic dynamics of activation in cardiac Purkinje fibers. *Circ. Res.* 66, 525–545.
- Cohen, C., Fozzard, H., Sheu, S.S., 1982. Increase in intracellular sodium ion activity during stimulation in mammalian cardiac muscle. *Circ. Res.* 50, 651–662.

<sup>17</sup>Another argument against letting  $\tau_{\text{open}} \rightarrow \infty$  derives from the limited range of the DI in Fig. 4a,  $D_{\text{ss}} \leq 400$  ms. Equation (9) captures the fact that, typically in experiments,  $S_{12}$  has exponential decay at very large values of DI, but the simplified version (A.22) does not.

- Elharrar, V., Surawicz, B., 1983. Cycle length effect on restitution of action potential duration in dog cardiac fibers. *Am. J. Physiol.* 244, H782–H792.
- Fenton, F.E., Cherry, H.H., Evans, S., 2002. Multiple mechanisms of spiral wave breakup in a model of cardiac electrical activity. *Chaos* 12, 852–892.
- Fox, J.J., Bodenschatz, E., Gilmour, R.F., Jr., 2002a. Period-doubling instability and memory in cardiac tissue. *Phys. Rev. Lett.* 89, 1381011–1381014.
- Fox, J.J., Gilmour, R.F., Bodenschatz, E., 2002b. Conduction block in one dimensional heart fibers. *Phys. Rev. Lett.* 89, 198101–198104.
- Fox, J.J., McHarg, J.L., Gilmour, R.F., Jr., 2002c. Ionic mechanism of electrical alternans. *Am. J. Physiol.* 282, H516–H530.
- Fox, J., Riccio, M., Drury, P., Werthman, A., Gilmour, R., 2002d. Dynamic mechanism for conduction block in heart tissue. *New J. Physics* 5, 10111–10114.
- Gilmour, R., Otani, N., Watanabe, M., 1997. Memory and complex dynamics in cardiac Purkinje fibers. *Am. J. Physiol.* 272, H1826–H1832.
- Greenstein, J., Winslow, R., 2003. An integrative model of the cardiac ventricular myocyte incorporating local control of  $\text{Ca}^{2+}$  release. *Biophys. J.* 83, 2918–2945.
- Hall, G.M., Bahar, S., Gauthier, D.J., 1999. Prevalence of rate-dependent behaviors in cardiac muscle. *Phys. Rev. Lett.* 82, 2995–2998.
- Hund, T., Kucera, J., Otani, N., Rudy, Y., 2001. Ionic charge conservation and long-term steady-state in the Luo–Rudy dynamic cell model. *Biophys. J.* 81, 3324–3331.
- Kalb, S.S., 2004. Experimental and theoretical investigation of cardiac restitution and memory: A comprehensive approach using the restitution portrait. Ph.D. thesis, Department of Biomedical Engineering, Duke University, Durham, NC.
- Kalb, S.S., Dobrovolny, H.M., Tolkacheva, E.G., Idriss, S.F., Krassowska, W., Gauthier, D.J., 2004. The restitution portrait: a new method for investigating rate-dependent restitution. *J. Cardiovasc. Electrophysiol.* 15, 698–709.
- Karma, A., 1993. Spiral breakup in model equations of action potential propagation in cardiac tissue. *Phys. Rev. Lett.* 71, 1103–1107.
- Kobayashi, Y., Peters, W., Khan, S., Mandel, W., Karagueuzian, H., 1992. Cellular mechanisms of differential action potential duration restitution in canine ventricular muscle cells during single versus double premature stimuli. *Circulation* 86, 955–967.
- Koller, M., Riccio, M., Gilmour, R., 1998. Dynamic restitution of action potential duration during electrical alternans and ventricular fibrillation. *Am. J. Physiol.* 275, H1635–H1642.
- Luo, C., Rudy, Y., 1994. A dynamic model of the cardiac ventricular action potential. *Circ. Res.* 74, 1071–1096.
- Morad, M., Cleemann, L., 1987. Role of  $\text{Ca}^{2+}$  channel in development of tension in heart muscle. *J. Mol. Cell Cardiol* 19, 527–553.
- Mitchell, C.C., Schaeffer, D.G., 2003. A two-current model for the dynamics of cardiac membrane. *Bull. Math. Bio.* 65, 767–793.
- Nolasco, J.B., Dahlen, R.W., 1968. A graphic method for the study of alternation in cardiac action potentials. *J. Appl. Physiol.* 25, 191–196.
- Oliver, R.A., Wood, A.W., Kalb, S.S., Krassowska, W., 2004. Restitution Portrait in Luo-Rudy dynamic cardiac membrane model, in Proceedings of the 2004 Biomedical Engineering Society Annual Fall Meeting, Philadelphia, PA, pp. 16.
- Otani, N., Gilmour, R., 1997. Memory models for the electrical properties of local cardiac systems. *J. Theor. Bio* 187, 409–436.
- Schaeffer, D., Ying, W.J., Zhao, X.P., 2006. Derivation of a 2D mapping model with memory from an ionic model for cardiac restitution. *Nonlin. Dynam.* Manuscript submitted for publication.
- Shiferaw, Y., Sato, D., Karma, A., 2004. Subcellular Turing instability mediated by voltage and calcium diffusion in cardiac cells. Preprint.
- Shiferaw, Y., Watanabe, M.A., Garfinkel, A., Weiss, J.N., Karma, A., 2003. Model of intracellular calcium cycling in ventricular myocytes. *Biophys. J.* 85, 3666–3686.
- Tolkacheva, E., Romeo, M., Guerraty, M., Gauthier, D., 2004. Condition for alternans and its control in a two-dimensional mapping model of paced cardiac dynamics. *Phys. Rev. E* 69, 031904, 1–4.